Nanotechnology **20** (2009) 315501 (6pp) doi:10.1088/0957-4484/20/31/315501

Localized surface plasmon resonance detection of layered biointeractions on metallic subwavelength nanogratings

Kyujung Kim[1], Dong Jun Kim[2], Seyoung Moon[1], Donghyun Kim[1,2,4] and Kyung Min Byun[3]

[1] Program for Nanomedical Science and Technology, Yonsei University, Seoul 120-749, Korea
[2] School of Electrical and Electronic Engineering, Yonsei University, Seoul 120-749, Korea
[3] Department of Biomedical Engineering, Kyung Hee University, Yongin 449-701, Korea

E-mail: kimd@yonsei.ac.kr

Received 9 March 2009, in final form 4 June 2009
Published 13 July 2009
Online at stacks.iop.org/Nano/20/315501

Abstract
Enhanced detection of multiple targets such as self-assembled monolayer (SAM) formation, DNA hybridization, and ethanol ambient changes was explored using localized surface plasmon resonance (LSPR) excited by metallic surface nanogratings. The sensitivity enhancement depends on the target as well as the nanostructure with a maximum at 242% over a conventional structure when detecting an 11-mercaptoundecanoic acid SAM with an LSPR structure of 200 nm period. The measured enhancement shows smaller target-dependent variance when detecting various layered biointeractions, while structure-dependent variance was much larger. The result suggests the feasibility of the efficient detection of multiple biointeractions at enhanced sensitivity and extends the applicability of a nanostructured LSPR biosensor for diverse biomolecular events.

(Some figures in this article are in colour only in the electronic version)

1. Introduction

A surface plasmon (SP) is a longitudinal wave of electron concentration that is formed at a dielectric–metal interface when an incident transverse magnetic (TM) polarized photon is momentum matched for SP resonance (SPR). By measuring the resonance shift in response to molecular interactions on the metal surface, label-free sensing can be implemented on a quantitative basis in real time.

The sensitivity limit of traditional metal thin film-based SPR biosensors is of the order of 1 pg mm^{-2} [1]. Various approaches have been proposed to enhance the sensitivity of traditional SPR biosensors, e.g. signal amplification using functionalized nanoparticles [2], magneto-optic effects [3], surface relief nanostructure-mediated localized SPR (LSPR) [4–7], and phase-sensitive SPR detection schemes [8, 9].

Typically, localized SPs (LSPs) have been excited by colloidal metallic nanoparticles which showed a pronounced SPR angle shift by providing an additional mass during the binding process in a biomolecular interaction. In contrast, we have considered surface nanostructures on a metallic film as an alternative substrate whereby LSPs are excited. The LSPs interact with propagating SPs on the sensor surface and create hybrid modes. The dispersion relation between SP wavenumber k_{SP} and incident light angular frequency (ω) can be calculated from Maxwell's equations and is given by [10]

$$k_{SP} = \frac{\omega}{c}\sqrt{\frac{\varepsilon_m \varepsilon_d}{\varepsilon_m + \varepsilon_d}} \tag{1}$$

$$k_q = k_{SP} - qK_G = k_{air} n_p \sin\theta_{SPR} - q\frac{2\pi}{\Lambda} \tag{2}$$

where c, ε_m, ε_d, and n_p represent the speed of light, metal permittivity, dielectric permittivity, and refractive index of the prism substrate. In equation (2), θ_{SPR} and k_{air} are the angle of incidence at resonance and the wavenumber in free-space. K_G is the grating vector and is equal to $2\pi/\Lambda$ with Λ as

[4] Author to whom any correspondence should be addressed.

the grating period. q is an arbitrary integer that denotes a diffraction order. As the angle of qth diffracted light is given by $\theta_q^R = \sin^{-1}(k_q/n_p k_{air})$, for an LSPR biosensor with a period much smaller than the wavelength λ, $q = 0$ and only the zeroth diffraction order is valid and significant. To describe near-field excitation of localized plasmonic fields, ε_d may be replaced with the effective medium permittivity ε_{eff}, which is a complex number and can be dominantly negative real depending on the volume factor, which is the ratio of the volume occupied by metallic nanostructures per period. While one may use effective medium theories for subwavelength structures, in general, ε_{eff} and thus the dispersion relation of LSPs are not given in a closed form.

Use of nanogratings and nanoposts has produced significant signal enhancement in the case of surface nanostructure-based LSPR biosensors and plasmon enhanced total internal reflection fluorescence microscopy [6, 7, 11–14]. The enhancement depends on surface structures as well as molecular binding interactions. The dependence of the enhancement on the binding interaction itself has been the topic of a recent theoretical study [15]. The study confirms the sensitivity enhancement to be indeed a complex function of nanostructure design parameters and target binding interactions. There are three main factors that may be affecting the sensitivity characteristics of LSPR biosensors: index contrast provided by the specific biomolecular changes, conformation of the biomolecules under interaction, and the spatial distribution of field enhancement. The first two are derived from the target and are responsible for the target-related variation, while the last one describes the effect of nanostructures and is affected by two major interaction mechanisms between resonantly excited LSP modes: (1) interaction of propagating SPs in a metal film and LSP modes in nanostructures and (2) LSP–LSP coupling between neighboring nanostructures [16].

In this paper, we intend to present the experimentally measured signal enhancement induced by surface relief nanostructures for detecting various targets. For this purpose, we used nanogratings of two different designs to measure the formation of a self-assembled monolayer (SAM) in water ambience and DNA hybridization in buffer solution. The SAM formation and DNA hybridization create a layer with an index contrast in the course of a molecular reaction. More specifically, DNA hybridization represents a target that is maintained in a layer and only its refractive index changes as a result of the interaction. In contrast, a SAM represents a target that forms a layer and thus changes both the thickness and the refractive index through the target interaction. For completeness, we compared our data with the results of varying ethanol concentration as these represent ambient changes, which do not form layers in the middle of or as a consequence of biochemical processes. It was theoretically suggested that the sensitivity enhancement of nanostructure-based LSPR would be lower when detecting ambient changes because of reduced index contrast [15].

2. Methods and materials

2.1. Numerical methods

The designs were numerically determined to produce enhanced sensitivity using rigorous coupled-wave analysis (RCWA) and the finite time domain (FDTD) method. RCWA has been successfully applied to describing optical characteristics of various nanostructures. If the media are assumed to be linear with respect to the electromagnetic fields, homogeneous, isotropic, time-invariant, and source-free, Maxwell equations are reduced to a generalized Helmholtz equation

$$\nabla^2 H_y(x,z) + k^2 n^2 H_y(x,z) = 0 \tag{3}$$

for TM polarized light. The refractive index $n = [\varepsilon(x,z)\mu(x,z)]^{1/2}$ and k is the wavenumber. Under a pseudo-periodic boundary condition, the Floquet–Bloch theorem is invoked as follows:

$$H_y(x,z) = H_y(x+\Lambda,z)\exp(\mathrm{i}\sin\theta) \tag{4}$$

for $0 < x < \Lambda$ and $-\infty < z < \infty$. θ denotes the angle of incidence. From general grating theory, the Rayleigh expansion holds as a solution of the field:

$$H_y(x,z) = \sum_{m=-\infty}^{\infty} A_m \exp(\mathrm{i}k_{xm}x + \mathrm{i}k_{zm}z) \tag{5}$$

where A_m is the appropriate reflection or transmission coefficient. The z dependence of the complex permittivity can be eliminated for an infinitely long, one-dimensional grating, thereby it is possible to express the solution inside the grooves as a Fourier expansion. The unknown reflection and transmission coefficients can be determined based on the continuity of the tangential components of the electromagnetic fields at the boundaries between media. Details of RCWA can be found elsewhere [17–19]. For the simulation presented in this study, 30 spatial harmonics have been employed, unless otherwise noted.

2.2. Device fabrication

We fabricated four working samples of two different nanograting designs (A and B), as listed in table 1. A gold film with thickness d_f was first evaporated on an SF10 slide glass substrate after an evaporation of a 2 nm thick chromium adhesion layer. A grating pattern was then defined by electron beam lithography on a PMMA photoresist layer, followed by evaporation of gold (thickness: d_g). The pattern was transferred to form a metal grating by lift-off. Figure 1 shows scanning electron microscope images of samples A and B that confirm the nanograting patterns fabricated as designed. Note that nanostructures in this study are based on 2D nanogratings because of the relative ease of modeling and fabrication, compared to more complex 3D structures such as nanoposts or nanoholes. The general trends of sensitivity enhancement, though, may remain valid in LSPR based on complex nanostructures.

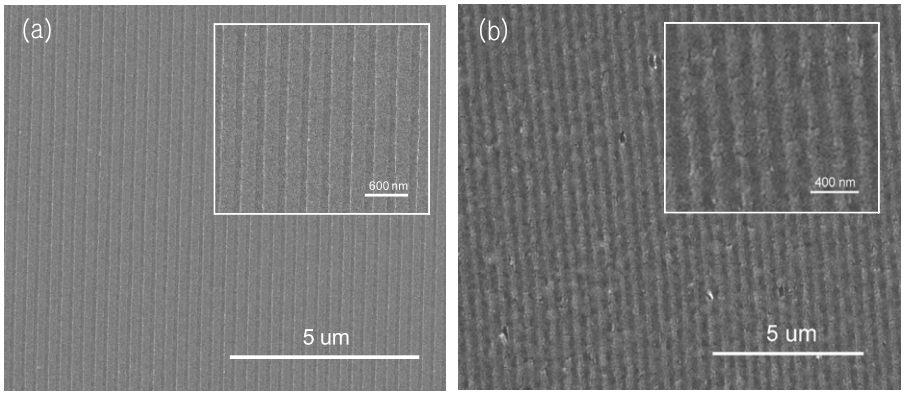

Figure 1. Scanning electron microscope image of the fabricated nanograting (a) A and (b) B. The inset shows a magnified image.

Table 1. Parameters of the fabricated samples.

	d_f (nm)	d_g (nm)	Λ (nm)	Target
A1	55	10	300	DNA hybridization
A2				SAM formation
B1	40	15	200	
B2				Ethanol ambience[a]

[a] Taken from [6].

2.3. Optical set-up

We used a custom-made optical set-up to measure SPR signals, as shown in figure 2. The set-up was based on dual concentric motorized rotation stages (URS75PP, Newport, Irvine, CA) for angle scanning measurement with a nominal angular resolution at 0.002°. The set-up employs a polarized 10 mW He–Ne laser ($\lambda = 0.6328$ μm, 25-LHP-991, Melles-Griot, Carlsbad, CA) as a light source and a calibrated photodiode (818-UV, Newport, Irvine, CA) as a photodetector. Due to the angle scanning, the set-up does not measure an interaction in real time. This is not a serious concern as far as this study is concerned, since we are interested only in the net resonance shift before and after an interaction, not details of intermediate kinetics. The minimum detectable refractive index of the set-up is estimated to be $\Delta n \sim 1 \times 10^{-6}$ without any enhancement. Multiple (typically five) sites in a given sample were measured by translating the sample spatially to ensure consistency and thereby to reduce the standard variation. Measured resonance angles were in general consistent with numerical results using RCWA.

2.4. SAM and DNA preparation protocols

Protocols used in this study for SAM and DNA are as follows. The DNA hybridization process was first measured using sample A in table 1. Complementary 24-mer oligonucleotides (ss1; CACTGTCGGTATGCATGCCATGGC, and ss2; GCCATGGCATGCATACCGACAGTG) modified with thiol at 5′ end (Bioneer Co., Daejeon, Korea) were dissolved in distilled water to 100 pM μl^{-1}. 40 μl of ss2 was pipetted onto a gold nanograting chip and kept at 5 °C for adhesion. The chip was retrieved from the refrigerator after 24 h and washed with distilled water for up to 1 min to remove any un-immobilized target ssDNA. The chip was then index matched to a prism of the optical set-up. 40 μl of ss1 was added to 1 ml of hybridization buffer and thoroughly mixed. The hybridization process was controlled with a micropump (KD Scientific Inc., Holliston, MA) at 400 ml h^{-1}. Figure 3 shows the morphology of dsDNA formed on a nanograting sample. Although local variation may exist, the coating of DNA appears to be uniform over the area of the beam spot.

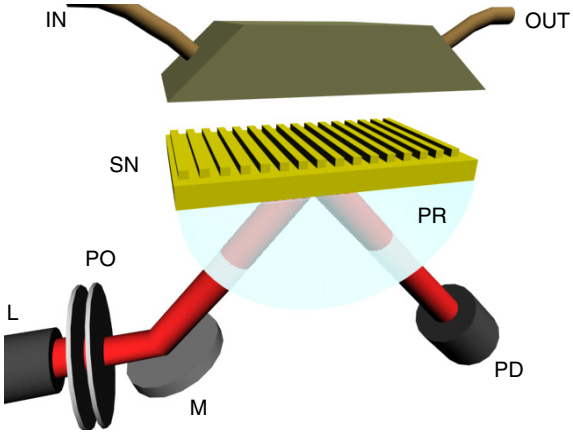

Figure 2. Schematics of the optical set-up and the mount of an LSPR assay (IN: inlet, L: laser, M: mirror, OUT: outlet, PD: photodetector, PO: polarizer, PR: prism, and SN: surface nanograting; not scaled).

The 11-mercaptoundecanoic acid (MUA), 95% (45056 Sigma-Aldrich Chemical Co., St Louis, MO) was employed to immobilize a SAM. First, the MUA was dissolved in an absolute 99.8% ethanol solution (Merck & Co. Inc., Whitehouse Station, NJ, USA) according to the procedure described from Aldrich. After that, the samples were immersed into MUA in an ethanol solution for about a day at room temperature. The modified samples were rinsed with ethanol and distilled water.

3. Results and discussion

The overall enhancement of nanostructure-based LSPR relative to conventional SPR was evaluated by the sensitivity enhancement factor (SEF), defined as the ratio of resonance

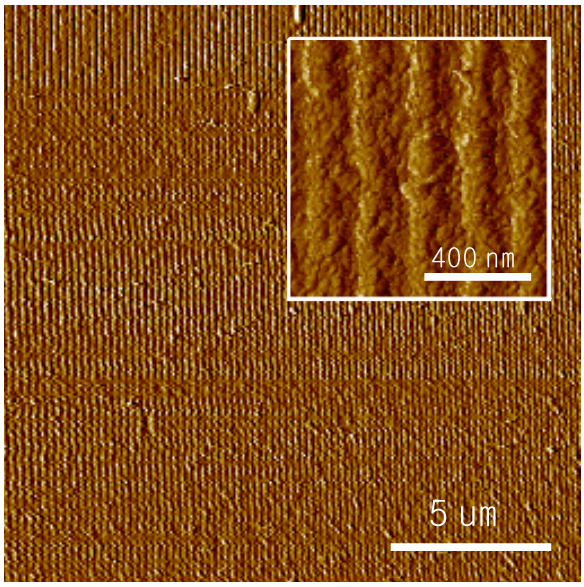

Figure 3. Atomic force microscope (AFM) image of dsDNA on a nanograting sample of $\Lambda = 200$ nm.

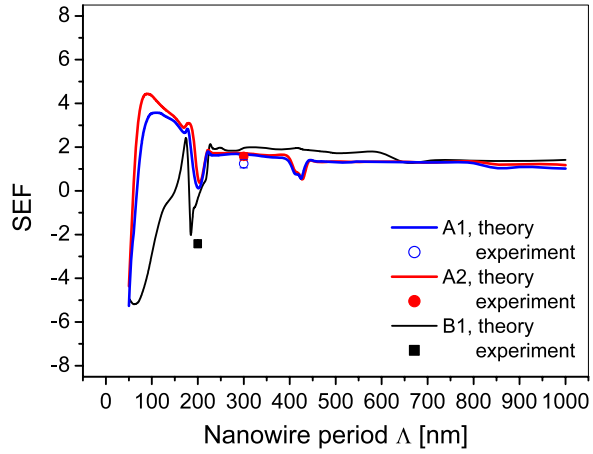

Figure 4. Sensitivity enhancement numerically calculated (lines) and experimentally obtained with the various nanograting listed in table 1 (symbols).

angle shift by the target on a nanostructure-based LSPR sample ($\Delta\theta_{\mathrm{LSPR}}$) to that on a control sample with no nanostructure ($\Delta\theta_{\mathrm{control}}$), i.e. SEF $= \Delta\theta_{\mathrm{LSPR}}/\Delta\theta_{\mathrm{control}}$.

SEF may be negative, which is associated with phase retardation by LSP excitation and the effect of damping induced by strong index contrast in the dispersion relation. The concept of negative shift was reported as early as in the 1970s, when it was dubbed as backbending [20, 21]. In the case of using a nanograting substrate with a small pitch and extreme fill factors, damping-related backbending of plasmon momentum kicks in, which induces the resonance momentum to be smaller with an interaction, although in a way complicated by the presence of subwavelength nanostructures [16]. Such a negative shift of resonance was observed experimentally in an LSPR biosensor using nanoparticles [2, 22]. From a functional perspective, it is only the magnitude of SEF that matters.

In our study, the highest SEF was obtained as 242% for detecting a SAM on the sample B. What should be noted is the variation of the sensitivity enhancement in that an LSPR sample may produce different outcomes for different targets. When target ssDNA is bound to a complementary sequence immobilized on the sensor surface, only a change of refractive indices may occur. On the other hand, SAM attachment induces the target thickness variation as well as refractive index change, which can influence its SEF by a different enhancement mechanism. In our results, DNA hybridization on sample A produced SEF $=$ 124% while SEF $=$ 157% for detecting a MUA SAM on the same sample. The variance ΔSEF/SEF $=$ 26.6%. We contrast this to the results with B. With sample B, detection of a MUA SAM produced SEF $=$ 242% and it was 144% when detecting ethanol variation (0–5%) in ambient atmosphere, i.e. the variance is 68.1%, significantly larger than that of A. Larger SEF difference in sample B is attributed to the fact that the ethanol test measures a bulk sensitivity, while SAM and DNA experiments are associated with a surface sensitivity. As the surface sensitivity represents a more practical performance measure of an SPR-based biosensor chip, a concentration change in ethanol solution would be disregarded in subsequent results.

Note that surface-roughness-related degradation might have affected the sensitivity enhancement, particularly in the case of sample B. The influence of the destructive interaction between plasmons in the rough surface on the sensitivity degradation was found not to be substantial for nanowires with $\Lambda \geqslant 200$ nm, so that the degradation in the sensitivity enhancement may be fairly limited [23].

Figure 4 compares measured SEFs with numerical calculation by RCWA assuming the thickness of SAM and DNA to be 2 and 8 nm, respectively. DNA hybridization was modeled by assuming n(ssDNA) $=$ 1.449 138 and n(dsDNA) $=$ 1.516 575 [24]. Also, n(MUA SAM) $=$ 1.45 [25]. From the theoretical results for A1 and A2, the enhancement achieved by a nanostructured LSPR sample tends to be uniform as long as it measures biomolecular interactions that form a layer. Note also that the structure-dependent variance is much larger than the target-dependent variance, as represented by the stark differences between SEFs of A and B for the same MUA SAM. This suggests that if a nanostructure is optimized for a reference target, it may perform almost equally well for optically similar biointeractions.

The uniform sensitivity enhancement, which we observed when measuring different layered biointeractions with a nanostructured LSPR assay, is associated with optical similarity of the biointeractions and field penetration depth. A rough estimate of the optical signature as a result of a biointeraction is the effective index contrast which is the index contrast weighted by the penetration depth and given by

$$D = \int_0^d \Delta n \mathrm{e}^{-z/p}\,\mathrm{d}z \approx \frac{\Delta n}{p}(1 - \mathrm{e}^{-dp}), \qquad (6)$$

where d and p denote the layer thickness and penetration depth. Δn is the index contrast by the interaction. In our work,

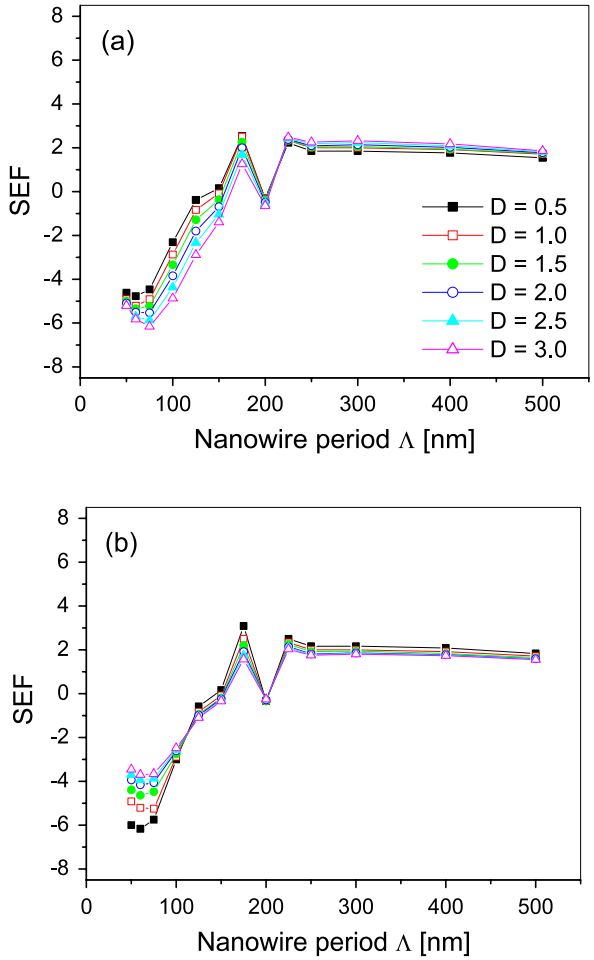

Figure 5. SEF calculated for various nanogratings as a function of effective index contrast D relative to that of a 2 nm thick MUA SAM ($n = 1.45$): (a) n varied, $d = 2$ nm, and (b) $n = 1.45$ and d varied.

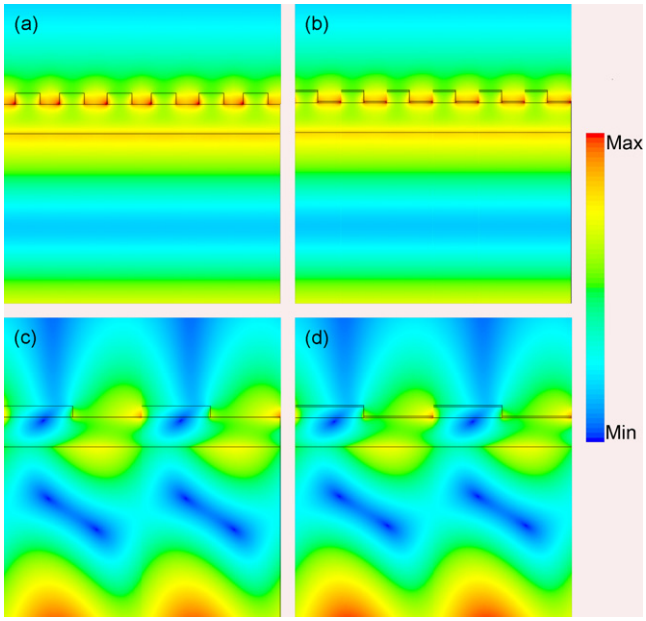

Figure 6. Field profiles ($|H_y|$) calculated by the FDTD method: (a) no SAM and (b) with a MUA SAM at $\Lambda = 60$ nm and same with (c) and (d) at $\Lambda = 200$ nm.

the ratio of D for DNA hybridization relative to a MUA SAM is approximately 2.2 for typical penetration depths. In other words, the optical signal of DNA hybridization is 2.2 times stronger than that of detecting the formation of a MUA SAM. Yet, the measured sensitivity enhancement came out relatively uniform.

We now turn to the range of D, in which the sensitivity enhancement remains uniform. Figure 5 shows SEF with D. D is varied in two ways, by changing the thickness of an interaction layer as its refractive index is fixed at 1.45 or by varying its refractive indices for $d = 2$ nm, so $D = 1$ represents the case of measuring a MUA SAM. It was found that SEF changes linearly with D such that the absolute SEF is larger with an increased D. For $\Lambda > 200$ nm, the variance was maintained to be smaller than 10%. The variance increased for small $\Lambda < 150$ nm, yet was still smaller than 30%. An exception was the structure with $\Lambda = 150$ nm, in which case the variance was as high as 112%. This is associated with inducing a slight sensitivity enhancement at the period related to the damping characteristics of the LSPR structure. Such a structure can be avoided with optimization prior to fabrication.

It should also be emphasized that SEF characteristics show smaller variance when layer thickness is varied. For grating periods ranging from 100 to 200 nm, the distribution of SEFs in figure 5(b) is found to be more concentrated. Therefore, in terms of SEF uniformity, nanograting-based SPR structures can be advantageous to multiple ligand bindings, e.g. antibody–antigen interaction and streptavidin–biotin reaction, which can construct a thicker target layer, compared with DNA or RNA hybridization, causing the concentration of biomolecules to be increased within a limited depth of binding.

As an additional note, figure 4 indicates that an LSPR sample with smaller nanograting period would in general perform better in terms of sensitivity and that experimental data agree well with numerical results. Maximum SEF is expected to approach 6 for detecting a MUA SAM using nanogratings at $\Lambda = 60$ nm. Figure 6 clearly shows well-defined hot spots of $|H_y|$, calculated by the FDTD method, as LSPs are coupled between ridges for $\Lambda = 60$ nm. The enhanced field can thus amplify the optical signals of a biointeraction more effectively. In contrast, the profiles of $|H_y|$ at $\Lambda = 200$ nm do not show such enhanced fields, since the couplings of the LSPs excited in neighboring nanograting ridges are weak. In both cases, $d_f = 40$ nm and $d_g = 15$ nm. A nanoimprinting technique can be used to produce the nanostructures on a commercial scale.

4. Concluding remarks

We have presented the sensitivity characteristics of LSPR biosensors based on periodic nanostructures. Target-dependent variance of the enhanced surface sensitivity was found to be fairly small, while the performance variance associated with surface nanostructures is quite significant. Under typical conditions of biointeractions, the variance was smaller than 30%. The maximum SEF obtained with an LSPR biosensor

at $\Lambda = 200$ nm was 242% for detecting a MUA SAM and can be higher with a smaller period.

The results presented in this paper suggest that once an LSPR structure is optimized for a target to produce enhanced sensitivity, the LSPR-based assay may be used for the detection of other layered interactions. The extended applicability is useful in rapid and efficient screening applications, in which numerous optically similar biointeractions should be measured, and also in applications that require repeated use of a single bioassay.

Acknowledgments

The authors acknowledge Shin Ae Kim and Young Wook Chang for taking AFM measurements and the support of the Korea Science and Engineering Foundation (KOSEF) through the National Core Research Center for Nanomedical Technology (R15-2004-024-00000-0), KOSEF M10755020003-08N5502-00310, and R01-2007-000-20821-0 funded by the Korean government (MEST). This work was also supported by the 'System IC 2010' project of the Ministry of Knowledge Economy and by the MEMS Research Center for National Defense funded by the Defense Acquisition Program Administration under 2009-MM-41-UD090024FD. K M Byun is grateful for the support of the Korea Research Foundation Grant funded by the Korean Government (MOEHRD, Basic Research Promotion Fund) (KRF-2008-331-D00229). K Kim was supported by the 2008 Seoul Fellowship program.

References

[1] Campbell C T and Kim G 2007 *Biomaterials* **28** 2380–92
[2] He L, Musick M D, Nicewarner S R, Salinas F G, Benkovic S J, Natan M J and Keating C D 2000 *J. Am. Chem. Soc.* **122** 9071–7
[3] Sepúlveda B, Calle A, Lechuga L M and Armelles G 2006 *Opt. Lett.* **31** 1085–7
[4] Byun K M, Kim S J and Kim D 2005 *Opt. Express* **13** 3737–42
[5] Kim K, Yoon S J and Kim D 2006 *Opt. Express* **14** 12419–31
[6] Byun K M, Yoon S J, Kim D and Kim S J 2007 *Opt. Lett.* **32** 1902–4
[7] Malic L, Cui B, Veres T and Tabrizian M 2007 *Opt. Lett.* **32** 3092–4
[8] Wu S Y, Ho H P, Law W C, Lin C and Kong S K 2004 *Opt. Lett.* **29** 2378–80
[9] Markowicz P P, Law W C, Baev A, Prasad P N, Patskovsky S and Kabashin A 2007 *Opt. Express* **15** 1745–54
[10] Raether H 1988 *Surface Plasmon on Smooth and Rough Surfaces and on Gratings* (Berlin: Springer) chapter 6
[11] Lakowicz J R 2005 *Anal. Biochem.* **337** 171–94
[12] Enderlein J and Ruckstuhl T 2005 *Opt. Express* **13** 8855–65
[13] Burghardt T P, Charlesworth J E, Halstead M F, Tarara J E and Ajtai K 2006 *Biophys. J.* **90** 4662–71
[14] Kim K, Kim D J, Cho E-J, Suh J-S, Huh Y-M and Kim D 2009 *Nanotechnology* **20** 015202
[15] Yoon S J and Kim D 2008 *J. Opt. Soc. Am.* A **25** 725–35
[16] Kim D 2006 *J. Opt. Soc. Am.* A **23** 2307–14
[17] Moharam M G and Gaylord T K 1982 *J. Opt. Soc. Am.* **72** 1385–92
[18] Moharam M G and Gaylord T K 1986 *J. Opt. Soc. Am.* A **3** 1780–7
[19] Van der Aa N P and Mattheij R M M 2007 *J. Opt. Soc. Am.* A **24** 2692–700
[20] Arakawa E T, Williams M W, Hamm R N and Ritchie R H 1973 *Phys. Rev. Lett.* **31** 1127–9
[21] Alexander R W, Kovener G S and Bell R J 1974 *Phys. Rev. Lett.* **32** 154–7
[22] Lyon L A, Pena D J and Natan M J 1999 *J. Phys. Chem.* B **103** 5826–31
[23] Byun K M, Yoon S J, Kim D and Kim S J 2007 *J. Opt. Soc. Am.* A **24** 522–9
[24] Elhadj S, Singh G and Saraf R F 2004 *Langmuir* **20** 5539–43
[25] Silin V, Weetall H and Vanderah D J 1997 *J. Colloid Interface Sci.* **185** 94–103